

High photon-number efficiencies with a fast 28-pixel parallel SNSPD

LORENZO STASI^{1,2,†,*}, TOWSIF TAHER^{2,†,*}, GIOVANNI V. RESTA¹,
HUGO ZBINDEN², ROB THEW² AND FÉLIX BUSSIÈRES¹

¹*ID Quantique SA, CH-1227 Genève, Switzerland*

²*Group of Applied Physics, University of Geneva, CH-1211 Genève, Switzerland*

[†]*The authors contributed equally to this work.*

*lorenzo.stasi@idquantique.com

*towsif.taher@unige.ch

Abstract: Since their inception, superconducting nanowire single-photon detectors have been enabling quantum optical applications and the rise of the photonic quantum industry. The evolution in the detector design and read-out strategies has led to the introduction of devices with a plurality of independent pixels, which have been able to operate with high system detection efficiency at high speed while also supporting photon number resolution capabilities. However, this comes at the cost of a complex readout that requires one coaxial cable for each pixel of the array. Here, we report a 28-pixel SNSPD with a dedicated parallel architecture that, while maintaining a simple readout with a single coaxial line, enables the detector to operate at high speed with low-performance degradation. The device shows a maximum single-photon efficiency (SDE) of 88% and is able to maintain its SDE above 50%, coupled with a timing jitter lower than 80 ps, up to a detection rate of 200 million counts per second (Mcps). The detector also provides state-of-the-art PNR performances with a 2-photon efficiency of 75% and a 3-photon efficiency of 60%.

1. Introduction

Single photons can be employed in applications ranging from quantum communication to photonic quantum computing and quantum-enhanced imaging and sensing [1]. The foreseen development of optical quantum computers and quantum networks will require generation, manipulation, and detection of quantum light, and in this context, distribution of entanglement using single-photons as flying qubits is paramount [2, 3]. The unprecedented capabilities that would result from the deployment of these technologies have driven the research community to push the limits of the performances for the fundamental components of such systems, namely single-photon sources [4–6], photonic integrated circuits [7, 8], quantum memories [9] and single photon detectors [10, 11]. In the case of single-photon detectors, near-unitary efficiency, few dark counts, low jitter, high detection rates, and photon-number resolution (PNR) will be required. In particular, the ability to resolve photon-number states is an essential functionality for different applications such as quantum repeater protocols [12], generation and distribution of heralded multi-photon entanglement [13–15], improved heralded single-photon sources [16–18], gaussian boson sampling [19, 20], linear optical quantum computing [21–23] and enhanced quantum metrology [24, 25]. Without a scalable solution for a device that can perform single-photon detection and PNR discrimination with high n -photon efficiencies [26] at high speed, QKD protocols, quantum networks, and optical quantum computers will suffer from severe speed limitations, hindering these technologies from achieving their full potential.

Amongst the wide variety of single-photon detectors, single-pixel superconducting nanowire single-photon detectors (SNSPDs) [27] have demonstrated remarkable results in terms of system detection efficiency (SDE) [28, 29], dark counts [30], timing jitter [31, 32] and capability to work at a wide range of wavelengths [33, 34]. Crucially, in their single-pixel implementation, these nanowires are limited by their recovery time of a few tens of nanoseconds [35, 36] and

cannot detect single-photon events faster than a few million counts per second (Mcps), without a sharp degradation of their efficiency and timing jitter [37]. The degradation of SDE and jitter drastically impacts the intrinsic PNR capability of such single-pixel SNSPDs, as low jitter and high SDE are required in order to have high n -photon efficiencies [38–41]. Another limitation to the use of single-pixel SNSPDs is that the PNR functionality can only be used with light pulses of a few tens of picoseconds at most [39–41], thus preventing their use in applications with light sources that produce photons with longer pulse durations [42].

To overcome the shortcomings of the single-pixel design, approaches based on time-multiplexing [43, 44] or spatial-multiplexing have been adopted [13, 45–48]. In the time-multiplexing approach, fiber loops and optical beam splitters are used to distribute the photons in different temporal bins, thus allowing discrimination of different photon-number states by a single-pixel SNSPD [44]. This scheme suffers from the additional losses of the optical beam splitters and fiber loops and is inherently slower than other approaches. Spatial-multiplexing can be exploited either by using multiple individual detectors and splitting the light with optical beam-splitters [13, 46–48] or by developing dedicated SNSPD designs, where the detection area is divided into several smaller SNSPDs (called pixels) that are biased and read-out individually [45]. The former approach does not address the speed limitation of single-pixel devices, and introduces additional losses due to the use of optical beam splitters. With the latter approach, the losses of the beam-splitters are removed, and it is possible to maintain high SDE at higher count rates and even reach maximum detection rates in the order of Giga-cps (Gcps) [49–51]. With these arrays, the photon-number information is encoded in the number of pixels that have clicked and a high number of pixels is necessary to minimize the probability that multiple photons are absorbed by the same pixel. However, this comes at the cost of a readout whose complexity scales linearly with the number of pixels. In fact, one coaxial cable per pixel is needed, and coincidence analysis has to be performed to extract information on the detected photon-number state, possibly limiting real-time operations. Crucially, the limited number of connections that can be made to the coldest stage of a cryo-cooler drastically limits the scaling of this architecture.

A solution to these limitations has been the development of a dedicated parallel architecture that allows one to combine the signal of the pixels of the SNSPD in parallel directly on-chip, thus allowing the use of a single cryogenic cable to read-out a parallel-SNSPD (P-SNSPD) [52]. This architecture also demonstrated PNR capabilities [16, 53], where the information on the detected photon-number state is encoded in the amplitude of the signal pulse. However, the small number of active pixels was limiting the maximum achievable detection rate (6 pixels, 100 Mcps detection rate with $\sim 35\%$ absolute efficiency) [52] and the photon-number efficiencies (4 pixels, 48% for 2-photon efficiency) [53].

In this work, we report the development of an optimized P-SNSPD architecture that allows for an increased number of pixels, thus enabling a unique combination of state-of-the-art performances and scalability. We demonstrate a 28-pixel P-SNSPD, with 88% SDE at the single photon level, that is able to reach 200 Mcps at 50% absolute SDE. The parallel architecture is able to maintain a timing jitter below 80 ps at a 200 Mcps detection rate while using a single coaxial line readout. We perform an in-depth analysis of the PNR performances of the device and demonstrate 2-photon efficiency of 75% and 3-photon efficiency of 60%. Finally, we compare our technology to other PNR methodologies, highlighting the strengths and shortcomings of each method in an effort to bring better clarity and understanding to a field that has seen rapid progress in recent years.

2. Device fabrication and characterization

The P-SNSPD consists of 28 nanowires fabricated on ~ 9 nm thick NbTiN layer, with ~ 100 nm width and ~ 100 nm spacing, arranged in an interleaved geometry to ensure uniform illumination of all pixels (Fig. 1a). The pixels are connected in parallel on-chip and read out with a single

coaxial cable. To avoid electrical cross-talk between the pixels due to the current redistribution effect after a photon-detection event, additional wider nanowires are connected in parallel to the active 28-pixels outside the illumination area of the fiber [52], as shown in Fig. 1b. The detector is integrated into an optical cavity designed for maximizing photon absorption at 1550 nm, coupled to an SMF-28 fiber with a self-aligning scheme [54], and placed in a closed cycle 3-stage cryostat (ID281, ID Quantique) at 0.8 K. We characterize the performance of the detector in terms of system detection efficiency (SDE), recovery time, count rate, and jitter.

The SDE as a function of the bias current is measured at 1550 nm by illuminating the P-SNSPD with a CW laser (Thorlabs MCLS1) at a photon flux of 10^5 photon/s (see Fig. 1c). The P-SNSPD shows a long plateau region of constant SDE, reaching a maximum SDE of 88% with only ~ 60 dark counts/s. Fig. 1d shows the normalized SDE as a function of time. The high number of active pixels (28) of our designs allows the efficiency to only drop by a value of $1/28^{\text{th}}$ after a single-photon detection, and their lower kinetic inductance allows for a fast recovery of the SDE. The SDE reaches 96% of its maximum value within 5 ns of a previous detection, and after 15 ns, the detector fully recovers. The shorter length of the individual nanowires, coupled with the presence of the plateau, helps us to select an operation current for the device that exhibits negligible thermal crosstalk between the pixels (see SI for details on thermal crosstalk analysis).

In Fig. 2a, we highlight a key advantage demonstrated by this architecture where a high detection rate is achieved by the P-SNSPD using only a single coaxial line read-out. We compare the evolution of the SDE of the P-SNSPD as a function of detection rate with a conventional single-pixel SNSPD fabricated on the same wafer. For the P-SNSPD detector, SDE remains above 80% up to 50 Mcps and above 50% up to 200 Mcps. We define the maximum count rate (MCR) as the detection rate at which the normalized efficiency decreases by 3 dB [50]. The detector demonstrates an MCR of ~ 250 Mcps, showing more than a 10-fold improvement with respect to the conventional single-pixel SNSPD that has an MCR of only ~ 20 Mcps.

We further study the suitability of our detector for applications in high-rate quantum key distribution (QKD), where detectors with Gcps detection rates are required to achieve high (~ 100 MHz) secret key rates. Such high detection rates have previously been realized using spatially multiplexed SNSPDs with independent biasing and read-out of each pixel as demonstrated in Ref. [55, 56], where detectors requiring 16 and 14 cryogenic read-out channels were used respectively. In Fig. 2a, we demonstrate Gcps detection rates using four P-SNSPD detectors requiring only four coaxial lines. To achieve this, we split the optical input using a commercially available 1:4 optical beam splitter and send the outputs of the splitter to four detectors with 88%, 86%, 85%, and 82% SDE, respectively. Each P-SNSPD is read out using one coaxial line (details on the measurement setup in SI). We achieve 1 Gcps detection rate at $\sim 45\%$ absolute SDE and a MCR of ~ 1.3 Gcps, with a much simpler read-out scheme compared to Ref. [49–51, 55]. With this method, achieving such extreme detection rates comes at the cost of losses that are introduced in the optical set-up by the 1:4 splitter (0.5 dB loss from manufacturer), connectors (0.1 dB), and mating sleeves (0.1 dB) limiting the maximum achievable SDE to $\sim 72\%$. We expect that by carefully selecting an ultra-low loss splitter and splicing the fibers, it would be possible to achieve $>80\%$ maximum SDE and $>50\%$ absolute SDE at 1 Gcps detection rate.

Another key metric for SNSPD performance is the timing jitter, which characterizes the uncertainty in the measured arrival time of a photon. A unique feature of this architecture is the capability to maintain low jitter with increasing count rate without employing any jitter correction methods such as differential readout [57] or time-walk correction [37]. To demonstrate this feature, we characterized the evolution of the detector jitter with respect to the detection rate by superimposing photons from a pulsed laser (NuPhoton Technologies, 27 MHz repetition rate, 6 ps pulse width) and a CW laser (Thorlabs, MCLS1) via a 50:50 beam splitter. The photons from the CW laser were used to achieve high detection rates, and the pulsed laser provided photons to characterize the jitter (details of the measurement set up in SI). Fig. 2b shows results from

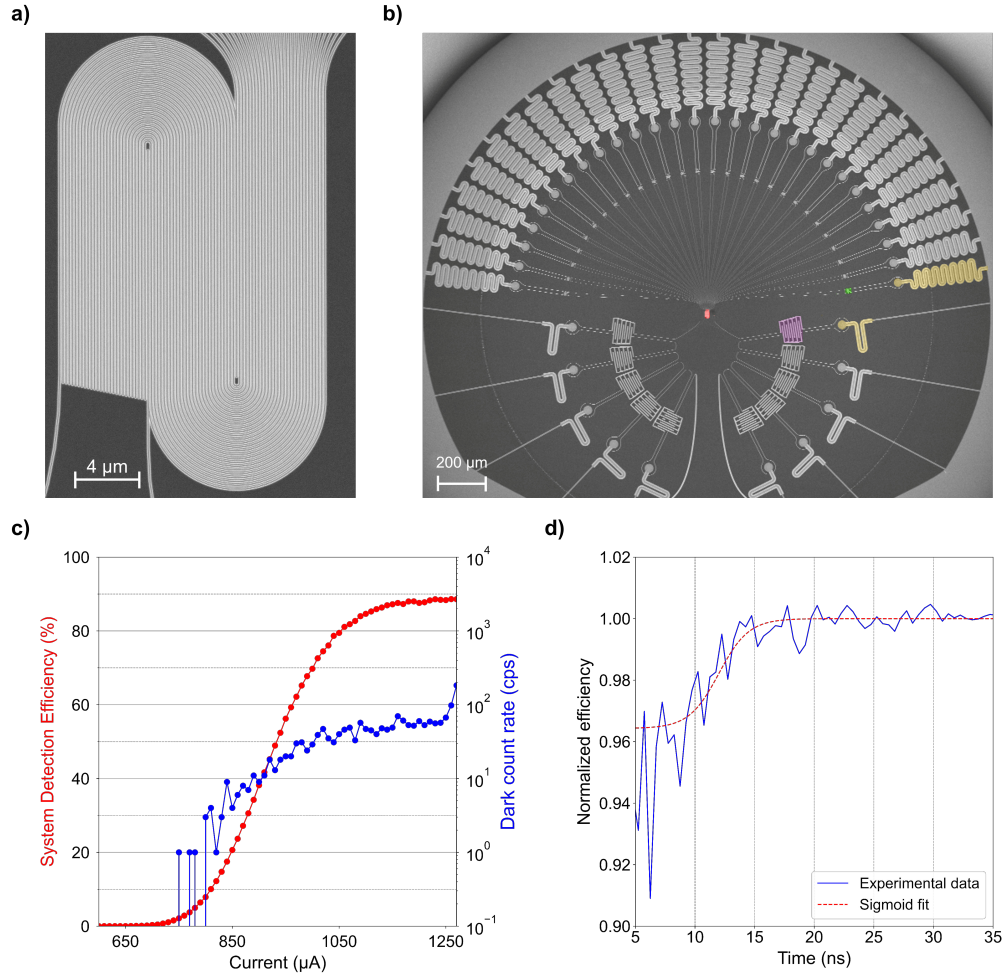


Fig. 1. **a)** SEM image of the active 28-pixels arranged in an interleaved geometry. The active area of the detectors is $\sim 225 \mu\text{m}^2$. **b)** Recolored SEM image of the entire parallel architecture. In the center, the 28 active nanowires are recolored in red. In the half-top part, there are meandered series resistors (yellow), ensuring a uniform bias of the pixels, and small series inductors (green), which tune the kinetic inductance of the pixels. In the bottom-half, there are the additional unexposed micro-wires (purple) and resistors (yellow), needed to avoid electrical crosstalk due to the current redistribution effect. **c)** System detection efficiency (red circles) and dark-count rate (blue circles) of the 28-pixels P-SNSPD measured with a 1550 nm CW laser at a photon flux of $\sim 10^5$ photon/s. **d)** Recovery of the detector efficiency as a function of time. The efficiency reaches 96% of its maximum value within 5 ns of a previous detection and fully recovers in less than 15 ns.

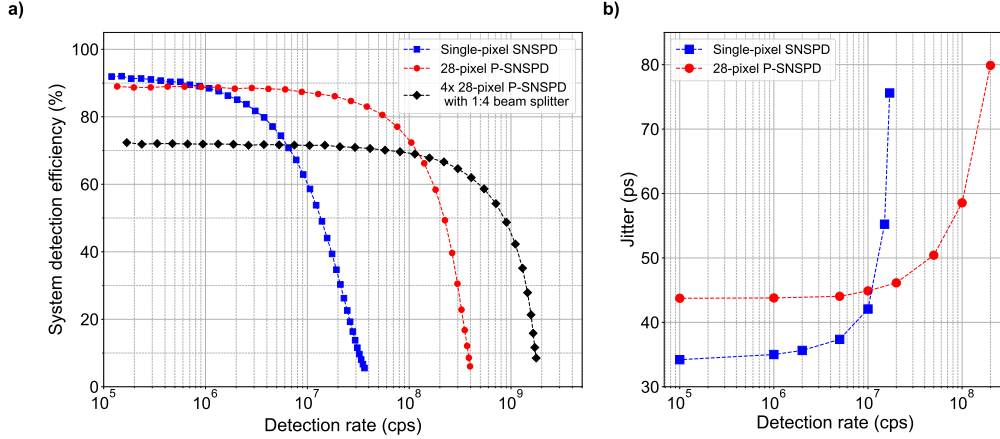


Fig. 2. **a)** SDE as a function of the detection rate measured with 1550 nm CW laser for a 28-pixel P-SNSPD (red circles), a standard single-pixel SNSPD (blue squares) and 4x 28-pixel P-SNSPD with optical beam-splitter (black diamonds). Note that for the 4x 28-pixel P-SNSPD, we used off-the-shelf components and did not factor out any losses. **b)** Timing jitter as a function of the detection rate for a 28-pixel P-SNSPD (red circles) and for a standard single-pixel SNSPD (blue squares).

this characterization for a P-SNSPD detector and the same conventional single-pixel detector as before. For our P-SNSPD, the jitter remains below 60 ps up to 100 Mcps and continues to stay below 80 ps until 200 Mcps, whereas, for the single pixel SNSPD, the jitter goes above 70 ps after 15 Mcps count rate.

3. Photon-number-resolution

In this section, we perform an in-depth study of the PNR performances of the detector. We further discuss the strengths and weaknesses of different photon number resolution methods, highlighting some key metrics that are of central importance for their operation.

3.1. Characterization of photon-number-resolution performance

In the P-SNSPD architecture, the individual pixels are electrically connected in parallel on-chip, and only a single coaxial-line is needed to read-out all pixels. This unique feature allows the information on the number of pixels that clicked to be encoded in the voltage amplitude of the output signal, as shown in Fig. 3a. Since the output signal is, to a first approximation, the sum of the contribution of each pixel, the amplitude of the n -click trace is roughly n times the 1-photon amplitude. However, this mechanism only works if the photons are arriving on the detector plane within the rise time of the electrical signal (~ 300 ps). For longer light pulses, the amplitudes might sum up in a non-trivial way, and no simple discrimination based on the voltage amplitude of the output can be achieved. For pulse duration below 300 ps, the clear separation between the n -click amplitudes leads to a unitary probability of assigning them to the corresponding n -click event (i.e. 100% assignment probability), as exemplified in Fig. 3b. By assigning the threshold levels for each n -click event within the shaded grey region in Fig. 3b, the corresponding n -photon counts can be extracted without any cross-talk between them, and without the use of time tagging devices with ps-level resolution. This is a great advantage compared to PNR schemes based on analysis of the rising/falling edge of a standard single-pixel SNSPD signal, where the probability of correctly assigning n -photon events rapidly decreases after 3-photons [38, 40, 41] and that can only be used with light pulses of a few tens of ps [39–41].

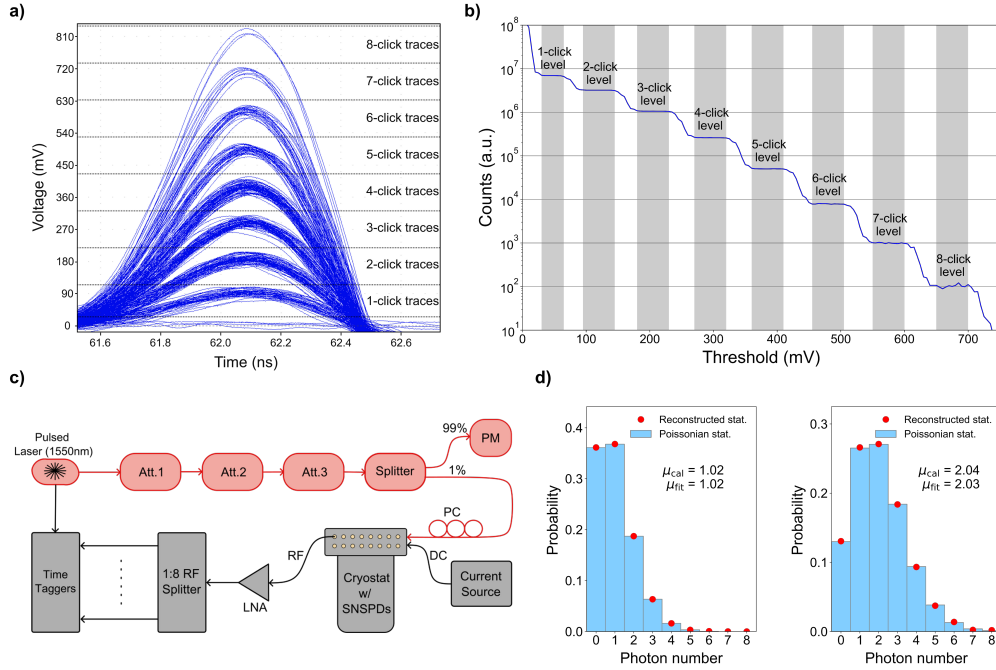


Fig. 3. **a)** Electrical voltage pulse generated by the P-SNSPD. **b)** Plot of counts as a function of threshold, where 8 well-separated regions can be identified. **c)** Schematic of the experimental setup to acquire the photon counting statistics (PM: Power meter; PC: Polarization controller; Att.: Optical attenuator). **d)** Coherent state reconstruction for μ equal to 1 and 2, performed with a 1550 nm pulsed laser at a rate of 40 MHz.

To describe the multi-photon response of the 28-pixel P-SNSPD, we use the model developed in Ref. [58] to construct the P_{nm} elements of the detector \mathbf{P} matrix, where P_{nm} is the probability of registering an n -click event when m photons are incident. Due to the low probability of dark counts, all the P_{nm} elements with $n > m$ are set to 0; thus, \mathbf{P} is an upper triangular matrix. These probabilities are necessary to link the photon-counting statistics, Q_n , namely the probability of measuring an n -click event by the PNR detector, to the incoming photon statistics, S_m , via $Q_n = \sum_{m=0}^{\infty} P_{nm} \cdot S_m$. In this formalism, the diagonal elements of the \mathbf{P} matrix (the P_{nn} elements) are known as n -photon efficiencies and are calculated as $\frac{N!}{(N-n)!} \left(\frac{\eta}{N}\right)^n$, where N is the number of pixels, n is the number of photons and η is the single-photon efficiency of the detector. This formula shows that when using spatial multiplexing, as it is the case for P-SNSPDs, the n -photon efficiencies are maximized by increasing N and η . With an increased number of pixels ($N \gg n$), the P-SNSPD approaches an intrinsic PNR behavior, where the P_{nn} are simply given by η^n . This point will be discussed further in the following sections.

To validate the model and to demonstrate the possibility of performing photon number resolution at a high count rate, we perform coherent state reconstruction using Poissonian light at a 40 MHz repetition rate (33 ps pulse width). A calibrated mean-photon-number per pulse (μ_{cal}) is sent to the detector and the Q_n is acquired by splitting the P-SNSPD electrical signal into 8 copies. Each one of them is connected to a time tagging device (ID Quantique, ID1000), and the proper voltage threshold is applied to get the different 8-click events (see Fig. 3c for a schematic representation of the experimental set-up). From Q_n , we reconstruct S_m and fit it to a Poissonian distribution to retrieve its mean-photon-number per pulse (μ_{fit}). As can be seen in Fig. 3d, there is an excellent agreement between μ_{cal} and μ_{fit} , thus supporting the correctness of the model

and a 2-photon efficiency (P_{22}) of 75% and a 3-photon efficiency (P_{33}) of 60% (see SI for the \mathbf{P} matrix). The coherent state reconstruction with 40 MHz repetition rate pulses demonstrates the capability of the P-SNSPD to operate as a PNR detector at high count rates, thanks to the high number of pixels and their fast recovery time. In contrast, other methods of photon number resolution such as TES (limited to kHz rates) [59] or PNR schemes based on single-pixel SNSPD (limited to a few MHz rates due to rapid decline of the detector efficiency and jitter at high rates, as shown in Fig. 2), would not have been able to operate at such high-speed, failing to properly reconstruct the input light.

3.2. Confidence in photon number discrimination

In the previous section, we validated the \mathbf{P} matrix model of the detector, showed high n -photon efficiencies, and performed a statistical state-reconstruction of Poissonian light. Here, we investigate in more detail the response of the 28-pixel P-SNSPD to single-shot measurements, where at each trial, we are interested in evaluating if the detector has correctly discriminated the input photon-number state. This assessment cannot be done without placing some assumptions on the statistics of the input light, and in the following discussion, we limit our analysis to one mode of a two-mode squeezed vacuum state, which exhibits thermal statistics, in the low- μ regime. This light is generally produced by probabilistic photon-pair sources based on spontaneous parametric down-conversion (SPDC) or spontaneous four-wave mixing (SFWM) processes [5]. Since the \mathbf{P} matrix provides information on all multi-photon detection events, it is used to answer the following question: “What is the probability that given an n -click event from the P-SNSPD, there were exactly n photons in the input state?”. We refer to these quantities as the *confidence* at n -photons (C_n), and they can easily be calculated using Bayes’ theorem:

$$C_n = \frac{P_{nn} \cdot S_n}{Q_n} = \frac{P_{nn} \cdot S_n}{\sum_{m=n}^{\infty} P_{nm} \cdot S_m}, \quad (1)$$

where the denominator is the statistics of the specific n -click event, and the numerator represents the subset of correct click-events for such Q_n . In Fig. 4a-c, we report the confidence values at 1, 2, and 3 photons for three different PNR detection schemes: an intrinsic PNR detector (*i.e.* the n -photon efficiencies scale as η^n), an array composed of 8 individual single-pixel SNSPDs with splitting of optical inputs, and a 28-pixel P-SNSPD. The SNSPD array with 8 individual detectors and split optical input represents a setup similar to the experiment described in Ref [48] where 48 independent single-pixel SNSPDs were used to realize 6 PNR detectors (8 single-pixel SNSPD for each PNR). We perform this analysis assuming a single photon SDE of 90% for all detectors, and for the latter configuration, we add 0.3 dB losses to emulate the optical beam splitter. As it can be seen from Fig. 4a-c, for our P-SNSPD, the confidence values at 1, 2, and 3 photons remain respectively within 1%, 3%, and 7% of the intrinsic PNR values and far outperform the 8-detector configuration.

Depending on the specific application that requires discrimination of the photon-number state, a different metric might become relevant, such as: “What is the probability that given an input state with >1 photon, there will be a >1 -click event registered?”. This probability is of great importance for any single-photon sources that suffer from multi-photon emissions [17, 18, 53], quantum communication and linear optic quantum computing protocols that rely on the capability to distinguish only between 1 and >1 photons [12, 60, 61]. We refer to this quantity as the *confidence at more than 1 photon* $C_{>1}$. In order to answer this question, we need to re-normalize the input light statistics, considering only the subspace of the distribution where there is more than 1 photon. Given the original distribution $\mathbf{S} = [S_0, S_1, S_2, \dots, S_m]$, the re-normalized statistics are:

$$\mathbf{S}' = \left[0, 0, \frac{S_2}{1 - S_1 - S_0}, \frac{S_3}{1 - S_1 - S_0}, \dots, \frac{S_m}{1 - S_1 - S_0} \right]. \quad (2)$$

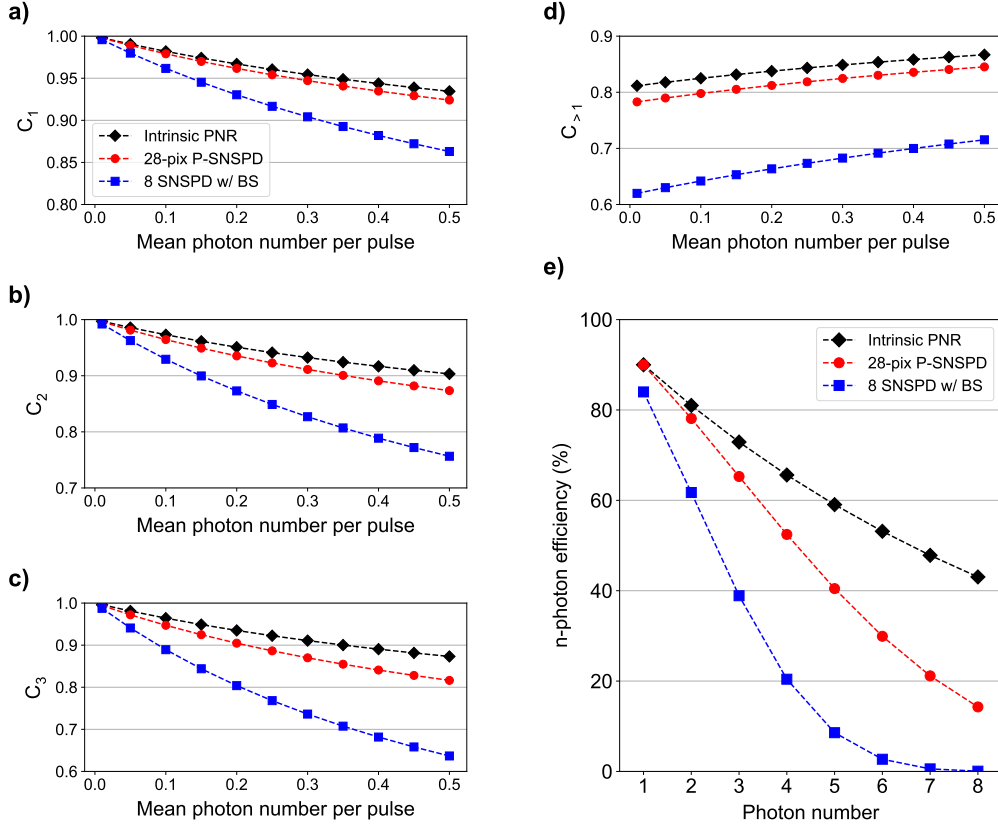


Fig. 4. **a) - d)** Plot of confidence at 1 photon (C_1) **a**, at 2 photons (C_2) **b**, at 3 photons (C_3) **c** and at more-than-one-photon ($C_{>1}$) **d** for an intrinsic PNR detector (black diamonds), a 28-pixel P-SNSPD (red circles) and a hypothetical configuration involving 8 standard SNSPD with an optical beam splitter (with 0.3 dB insertion loss) (blue squares). **e)** Scaling of the n -photon efficiencies for the aforementioned architectures.

Then, $C_{>1}$ can be expressed as:

$$C_{>1} = 1 - \sum_{m=2}^{\infty} P_{1m} \cdot S'_m - \sum_{m=2}^{\infty} P_{0m} \cdot S'_m, \quad (3)$$

where the second term represents the probability of registering a 1-click when more-than-1-photon is arriving on the detector, and the third term represents the probability of registering a 0-click event when more-than-1-photon is arriving on the detector. In Fig. 4d, we show the results for the same three PNR approaches. In this case, the P-SNSPD remains within 3% of the confidence values of an intrinsic PNR detector, while the 8 SNSPD configuration is considerably lower. As hinted above, the reason behind the drastic increase in performances enabled by the 28-pixel P-SNSPD lies in the improved n -photon efficiencies of the detector. In Fig. 4e, we present the n -photon efficiencies up to $n = 8$, for the intrinsic PNR detector, the 28-pixel P-SNSPD and the array composed of 8 individual single-pixel SNSPDs with splitting of optical input. There is less than 3% difference in the 2-photon efficiency and less than 8% difference for the 3-photon efficiency compared to an intrinsic PNR detector, while the performances of the 8 individual single-pixel SNSPDs with splitting of optical input are far from the intrinsic level. This analysis clearly shows the advantage that stems from the use of detectors with a high number of pixels.

3.3. Comparison of PNR approaches

With the following discussion, we aim to highlight some key metrics that can help to reliably evaluate and compare different schemes for photon-number resolution. Here, we define an ideal PNR detector as a device that should at least respect the following 2 properties:

- (i) the n -photon efficiencies should only depend on the single-photon efficiency of the detector, i.e. the diagonal elements of the \mathbf{P} matrix equal to η^n (where η is the device efficiency and n the photon number);
- (ii) the probability to assign each different output signal to the corresponding n -click event should be unitary in the range of interest (i.e. assignment probability of 1);

Together with these properties, we also highlight some key features that would be required by most practical applications:

- (a) absence of a strict limitation on the duration of the input light pulses;
- (b) ability to work at high count rates;
- (c) scalability of the read-out architecture and operational simplicity.

We focus our discussion on the five most commonly deployed methods for PNR at telecommunication wavelengths in literature: transition-edge sensors (TESs) [11, 59, 62], single-pixel SNSPDs with optical beam-splitters [13, 47, 48], analysis of rising/falling edge of single-pixel SNSPD signals [39–41], spatial multiplexing of SNSPD arrays in an independent readout configuration [49–51] and our P-SNSPD architecture.

Starting with TESs, they are known to possess intrinsic PNR capabilities due to their bolometric principle; thus, they satisfy requirements (i) and (a). To guarantee requirement (ii) up to high-photon number events [59], post-processing of the electrical pulses must be performed, and, since TESs usually display a slow recovery time, in the order of several hundreds of ns [59], this poses a severe limit to their operational speed. Combined with the complex cryogenics needed to reach the mK operating temperature, TESs fail to meet features (b) and (c).

A common approach to enable PNR capabilities with single-pixel SNSPDs has been to use a plurality of detectors and split the input optical signal, using lossy beam-splitters, amongst them [13, 47, 48]. In this approach, the requirement (i) cannot easily be met, as the number of multiplexed detectors is limited by the losses of the optical beam splitters and by the increased complexity of the read-out. In this configuration, the requirement (ii) is always met, and the detectors are able to perform PNR discrimination with light pulses of any duration, thus also satisfying (a). However, each single-pixel detector is still limited to low count rates, and it lacks scalability. Thus, this method fails to meet features (b) and (c).

A different approach relies on the analysis of the time difference in the electrical pulse rising/falling edge of the single-pixel SNSPD signals, which is impacted by the absorption of different photon numbers [39–41]. Analysis of the trace with a fast oscilloscope can also be used in this approach [40]. Though requirement (i) is satisfied, it becomes difficult to fulfill (ii): good discrimination between different photon-number events is achieved only up to 3-photon event, becoming more and more blurred with increasing photon-numbers. Moreover, this method requires detectors with extremely low jitter and time tagging devices with ps-level resolution, and it is limited to operation at a few MHz rate, thus making it extremely difficult to accomplish features (b) and (c). Lastly, this method is limited to a few-tens of ps light pulses at most since the different hotspots need to be generated at the same time [39–41], thus failing to meet feature (a). This method can be combined with using multiple detectors with optical beam-splitters, thus providing better PNR performances. It will, however, still suffer from the limitation highlighted above in terms of speed and read-out complexity.

SNSPD arrays with an independent read-out configuration have also been used as PNR detectors [49, 51]. With this implementation, requirement (i) cannot be fully reached; however, increasing the number of pixels can bring this scheme closer and closer to the ideal n -photon efficiencies. Requirement (ii) is always satisfied without the need for any post-processing of the electrical pulses, and the devices can work at high-detection rates (feature (b)) and with any light pulse duration (feature (a)). However, the need for 1 coaxial cable per pixel greatly improves the scalability of this technology, which fails to meet feature (c) and also puts a limit on the number of pixels that can be made on a single device (e.g., a single device with n independent pixels will require an entire n -channel cryostat).

The architecture presented here has a similar limitation compared to arrays with independent pixel read-out in terms of fulfilling requirement (i); however, with this method, almost ideal n -photon efficiencies can be reached by increasing the number of pixels without impacting the read-out complexity. As we showed in 3(b), the assignment probability for the parallel architecture is 1, thus completely fulfilling requirement (ii). Feature (a) and (b) are partially fulfilled since the P-SNSPD can work until a few hundred ps light pulses, and we demonstrate that it can operate until a 40 MHz rate. Finally, they require only 1 coaxial cable, regardless of the number of pixels that the device has, do not require high-precision time tagging devices, and can discriminate photon numbers in real-time, thus fulfilling (c) as the most scalable solution.

	n -photon efficiency scaling	Assignment probability > 95%	Operating repetition rate	Readout	Light pulse duration
TES [59]	η^n	Up to 14 photon	100 kHz	SQUID, trace digitalization	10s of ns
Rising/falling-edge analysis [40, 41]	η^n	Up to 3 photon	Few MHz	Time tagging with ps resolution or trace analysis	10s of ps
SNSPDs w/ BS [48]	$\frac{N!}{(N-n)!} \left(\frac{\eta}{N}\right)^n$	Yes	10s MHz	1 cable per detector and coincidence analysis	Any
Independent read-out arrays [51]	$\frac{N!}{(N-n)!} \left(\frac{\eta}{N}\right)^n$	Yes	~ 100 MHz	1 cable per pixel and coincidence analysis	Any
Parallel SNSPD [This work]	$\frac{N!}{(N-n)!} \left(\frac{\eta}{N}\right)^n$	Yes	40 MHz	1 cable and amplitude discrimination	100s of ps

Table 1. Performance and operational comparison of different approaches for PNR.

4. Conclusion

In conclusion, we present an optimized and scalable parallel SNSPD architecture suitable for diverse applications. We fabricate and characterize a 28-pixel P-SNSPD detector that, thanks to the parallel architecture, uses a single cryogenic read-out channel. The P-SNSPD shows an 88% SDE at the single-photon level and is capable of reaching 200 Mcps count rate at 50% absolute SDE coupled with a timing jitter at 200 Mcps of 80 ps. Using only four such detectors, with a total of four cryogenic read-out channels, we achieved a ~ 1.3 Gcps maximum count rate (MCR). The P-SNSPD also enables a simple approach based on the discrimination of the amplitude of its output voltage to achieve state-of-the-art photon-number capabilities. We report 75% 2-photon and 60% 3-photon efficiencies and perform accurate state reconstruction of Poissonian light at a repetition rate of 40 MHz. Finally, we provide an in-depth discussion of different PNR approaches, comparing their strengths and weaknesses. The combination of a scalable read-out, high efficiency, low jitter, and enhanced photon number resolution capabilities at high detection rates makes these detectors well-suited for quantum network applications and high-speed optical quantum computing protocols.

Acknowledgments. The authors acknowledge financial support from the Swiss NCCR QSIT, Innosuisse Grant 40740.1 IP-ENG, and from NRC CSTIP Grant QSP043. L.S. is part of the AppQInfo MSCA

ITN, which received funding from the EU Horizon 2020 research and innovation program under Marie Skłodowska-Curie Grant Agreement 956071.

Disclosures. The authors declare no conflicts of interest.

Data availability. Data underlying the results presented in this paper may be obtained from the authors upon reasonable request.

References

1. C. M. Natarajan, M. G. Tanner, and R. H. Hadfield, “Superconducting nanowire single-photon detectors: physics and applications,” *Supercond. science technology* **25**, 063001 (2012).
2. S. Slussarenko and G. J. Pryde, “Photonic quantum information processing: A concise review,” *Appl. Phys. Rev.* **6** (2019).
3. K. Azuma, S. E. Economou, D. Elkouss, *et al.*, “Quantum repeaters: From quantum networks to the quantum internet,” *Rev. Mod. Phys.* **95**, 045006 (2023).
4. N. Somaschi, V. Giesz, L. De Santis, *et al.*, “Near-optimal single-photon sources in the solid state,” *Nat. Photonics* **10**, 340–345 (2016).
5. E. Meyer-Scott, C. Silberhorn, and A. Migdall, “Single-photon sources: Approaching the ideal through multiplexing,” *Rev. Sci. Instruments* **91**, 041101 (2020).
6. N. Tomm, A. Javadi, N. O. Antoniadis, *et al.*, “A bright and fast source of coherent single photons,” *Nat. Nanotechnol.* **16**, 399–403 (2021).
7. J. Wang, F. Sciarrino, A. Laing, and M. G. Thompson, “Integrated photonic quantum technologies,” *Nat. Photonics* **14**, 273–284 (2020).
8. C. Wang, Z. Li, J. Riemensberger, *et al.*, “Lithium tantalate photonic integrated circuits for volume manufacturing,” *Nature* pp. 1–7 (2024).
9. C. Simon, M. Afzelius, J. Appel, *et al.*, “Quantum memories: a review based on the european integrated project “qubit applications (qap)”,” *The Eur. Phys. J. D* **58**, 1–22 (2010).
10. R. H. Hadfield, “Single-photon detectors for optical quantum information applications,” *Nat. photonics* **3**, 696–705 (2009).
11. A. E. Lita, D. V. Reddy, V. B. Verma, *et al.*, “Development of superconducting single-photon and photon-number resolving detectors for quantum applications,” *J. Light. Technol.* **40**, 7578–7597 (2022).
12. N. Sangouard, C. Simon, H. de Riedmatten, and N. Gisin, “Quantum repeaters based on atomic ensembles and linear optics,” *Rev. Mod. Phys.* **83**, 33–80 (2011).
13. H. Cao, L. M. Hansen, F. Giorgino, *et al.*, “Photonic source of heralded greenberger-horne-zeilinger states,” *Phys. Rev. Lett.* **132**, 130604 (2024).
14. F. J. Marcellino, P. Caspar, T. Brydges, *et al.*, “Toward heralded distribution of polarization entanglement,” *Opt. Quantum* **2**, 181–188 (2024).
15. T. Gerrits, S. Glancy, T. S. Clement, *et al.*, “Generation of optical coherent-state superpositions by number-resolved photon subtraction from the squeezed vacuum,” *Phys. Rev. A* **82**, 031802 (2010).
16. L. Stasi, P. Caspar, T. Brydges, *et al.*, “High-efficiency photon-number-resolving detector for improving heralded single-photon sources,” *Quantum Sci. Technol.* **8**, 045006 (2023).
17. S. I. Davis, A. Mueller, R. Valivarthi, *et al.*, “Improved heralded single-photon source with a photon-number-resolving superconducting nanowire detector,” *Phys. Rev. Appl.* **18**, 064007 (2022).
18. S. Sempere-Llagostera, G. Thekkadath, R. Patel, *et al.*, “Reducing $g^{(2)}(0)$ of a parametric down-conversion source via photon-number resolution with superconducting nanowire detectors,” *Opt. Express* **30**, 3138–3147 (2022).
19. J. M. Arrazola, V. Bergholm, K. Brádler, *et al.*, “Quantum circuits with many photons on a programmable nanophotonic chip,” *Nature* **591**, 54–60 (2021).
20. L. S. Madsen, F. Laudenbach, M. F. Askarani, *et al.*, “Quantum computational advantage with a programmable photonic processor,” *Nature* **606**, 75–81 (2022).
21. E. Knill, R. Laflamme, and G. J. Milburn, “A scheme for efficient quantum computation with linear optics,” *Nature* **409**, 46–52 (2001).
22. S. Bartolucci, P. Birchall, H. Bombin, *et al.*, “Fusion-based quantum computation,” *Nat. Commun.* **14**, 912 (2023).
23. N. Maring, A. Fyrrillas, M. Pont, *et al.*, “A versatile single-photon-based quantum computing platform,” *Nat. Photonics* pp. 1–7 (2024).
24. M. Von Helversen, J. Böhm, M. Schmidt, *et al.*, “Quantum metrology of solid-state single-photon sources using photon-number-resolving detectors,” *New J. Phys.* **21**, 035007 (2019).
25. M. Schmidt, M. Von Helversen, M. López, *et al.*, “Photon-number-resolving transition-edge sensors for the metrology of quantum light sources,” *J. Low Temp. Phys.* **193**, 1243–1250 (2018).
26. J. C. Bienfang, J. Bienfang, T. Gerrits, *et al.*, *Single-photon Sources and Detectors Dictionary* (US Department of Commerce, National Institute of Standards and Technology, 2023).
27. G. Gol’Tsmán, O. Okunev, G. Chulkova, *et al.*, “Picosecond superconducting single-photon optical detector,” *Appl. physics letters* **79**, 705–707 (2001).

28. D. V. Reddy, R. R. Nerem, S. W. Nam, *et al.*, “Superconducting nanowire single-photon detectors with 98% system detection efficiency at 1550 nm,” *Optica* **7**, 1649–1653 (2020).
29. J. Chang, J. Los, J. Tenorio-Pearl, *et al.*, “Detecting telecom single photons with 99.5- 2.07+ 0.5% system detection efficiency and high time resolution,” *APL Photonics* **6** (2021).
30. H. Shibata, K. Shimizu, H. Takesue, and Y. Tokura, “Ultimate low system dark-count rate for superconducting nanowire single-photon detector,” *Opt. letters* **40**, 3428–3431 (2015).
31. B. Korzh, Q.-Y. Zhao, J. P. Allmaras, *et al.*, “Demonstration of sub-3 ps temporal resolution with a superconducting nanowire single-photon detector,” *Nat. Photonics* **14**, 250–255 (2020).
32. I. Esmail Zadeh, J. W. Los, R. B. Gourgues, *et al.*, “Efficient single-photon detection with 7.7 ps time resolution for photon-correlation measurements,” *Acs Photonics* **7**, 1780–1787 (2020).
33. E. E. Wollman, V. B. Verma, A. D. Beyer, *et al.*, “UV superconducting nanowire single-photon detectors with high efficiency, low noise, and 4 K operating temperature,” *Opt. express* **25**, 26792–26801 (2017).
34. M. Colangelo, A. B. Walter, B. A. Korzh, *et al.*, “Large-area superconducting nanowire single-photon detectors for operation at wavelengths up to 7.4 μm ,” *Nano Lett.* **22**, 5667–5673 (2022).
35. I. Esmail Zadeh, J. W. Los, R. Gourgues, *et al.*, “Single-photon detectors combining high efficiency, high detection rates, and ultra-high timing resolution,” *Apl Photonics* **2** (2017).
36. C. Autebert, G. Gras, E. Amri, *et al.*, “Direct measurement of the recovery time of superconducting nanowire single-photon detectors,” *J. Appl. Phys.* **128** (2020).
37. A. Mueller, E. E. Wollman, B. Korzh, *et al.*, “Time-walk and jitter correction in snspds at high count rates,” *Appl. Phys. Lett.* **122** (2023).
38. C. Cahall, K. L. Nicolich, N. T. Islam, *et al.*, “Multi-photon detection using a conventional superconducting nanowire single-photon detector,” *Optica* **4**, 1534–1535 (2017).
39. D. Zhu, M. Colangelo, C. Chen, *et al.*, “Resolving photon numbers using a superconducting nanowire with impedance-matching taper,” *Nano Lett.* **20**, 3858–3863 (2020).
40. G. Sauer, M. Kolarczik, R. Gomez, *et al.*, “Resolving photon numbers using ultra-high-resolution timing of a single low-jitter superconducting nanowire detector,” *arXiv preprint arXiv:2310.12472* (2023).
41. T. Schapeler, N. Lamberty, T. Hummel, *et al.*, “How well can superconducting nanowire single-photon detectors resolve photon number?” *arXiv preprint arXiv:2310.12471* (2023).
42. T. Brydges, A. S. Raja, A. Gelmini, *et al.*, “Integrated photon-pair source with monolithic piezoelectric frequency tunability,” *Phys. Rev. A* **107**, 052602 (2023).
43. D. Achilles, C. Silberhorn, C. Sliwa, *et al.*, “Photon-number-resolving detection using time-multiplexing,” *J. Mod. Opt.* **51**, 1499–1515 (2004).
44. Y.-H. Deng, Y.-C. Gu, H.-L. Liu, *et al.*, “Gaussian boson sampling with pseudo-photon-number-resolving detectors and quantum computational advantage,” *Phys. review letters* **131**, 150601 (2023).
45. E. A. Dauler, B. S. Robinson, A. J. Kerman, *et al.*, “Multi-element superconducting nanowire single-photon detector,” *IEEE Trans. on Appl. Supercond.* **17**, 279–284 (2007).
46. N. Lusardi, J. Los, R. Gourgues, *et al.*, “Photon counting with photon number resolution through superconducting nanowires coupled to a multi-channel tdc in fpga,” *Rev. Sci. instruments* **88** (2017).
47. H. Wang, J. Qin, X. Ding, *et al.*, “Boson sampling with 20 input photons and a 60-mode interferometer in a 1 0 14-dimensional hilbert space,” *Phys. review letters* **123**, 250503 (2019).
48. M. J. Bayerbach, S. E. D’Aurelio, P. van Loock, and S. Barz, “Bell-state measurement exceeding 50% success probability with linear optics,” *Sci. Adv.* **9**, eadf4080 (2023).
49. W. Zhang, J. Huang, C. Zhang, *et al.*, “A 16-pixel interleaved superconducting nanowire single-photon detector array with a maximum count rate exceeding 1.5 GHz,” *IEEE Trans. on Appl. Supercond.* **29**, 1–4 (2019).
50. I. Craiciu, B. Korzh, A. D. Beyer, *et al.*, “High-speed detection of 1550 nm single photons with superconducting nanowire detectors,” *Optica* **10**, 183–190 (2023).
51. G. V. Resta, L. Stasi, M. Perrenoud, *et al.*, “Gigahertz detection rates and dynamic photon-number resolution with superconducting nanowire arrays,” *Nano Lett.* (2023).
52. M. Perrenoud, M. Caloz, E. Amri, *et al.*, “Operation of parallel SNSPDs at high detection rates,” *Supercond. Sci. Technol.* **34**, 024002 (2021).
53. L. Stasi, G. Gras, R. Berrazouane, *et al.*, “Fast high-efficiency photon-number-resolving parallel superconducting nanowire single-photon detector,” *Phys. Rev. Appl.* **19**, 064041 (2023).
54. A. J. Miller, A. E. Lita, B. Calkins, *et al.*, “Compact cryogenic self-aligning fiber-to-detector coupling with losses below one percent,” *Opt. express* **19**, 9102–9110 (2011).
55. W. Li, L. Zhang, H. Tan, *et al.*, “High-rate quantum key distribution exceeding 110 Mb s⁻¹,” *Nat. Photonics* **17**, 416–421 (2023).
56. F. Grünfelder, A. Boaron, G. V. Resta, *et al.*, “Fast single-photon detectors and real-time key distillation enable high secret-key-rate quantum key distribution systems,” *Nat. Photonics* **17**, 422–426 (2023).
57. M. Colangelo, B. Korzh, J. P. Allmaras, *et al.*, “Impedance-matched differential superconducting nanowire detectors,” *Phys. Rev. Appl.* **19**, 044093 (2023).
58. M. Fitch, B. Jacobs, T. Pittman, and J. Franson, “Photon-number resolution using time-multiplexed single-photon detectors,” *Phys. Rev. A* **68**, 043814 (2003).
59. L. A. Morais, T. Weinhold, M. P. de Almeida, *et al.*, “Precisely determining photon-number in real time,” *Quantum* **8**,

- 1355 (2024).
60. J. L. O'Brien, "Optical quantum computing," *Science* **318**, 1567–1570 (2007).
 61. T. C. Ralph and G. J. Pryde, "Optical quantum computation," in *Progress in optics*, vol. 54 (Elsevier, 2010), pp. 209–269.
 62. K. Irwin, "An application of electrothermal feedback for high resolution cryogenic particle detection," *Appl. Phys. Lett.* **66**, 1998–2000 (1995).